Climate Dynamics (2023) 61:1177–1192
https://doi.org/10.1007/s00382-022-06618-1

Mechanism of the summer rainfall interannual variability in transitional climate zone in East Asia: roles of teleconnection patterns and associated moisture processes

Qiulin Wang[1,2] · Lin Wang[1] · Gang Huang[3,4] · Ting Wang[5]

Received: 6 July 2022 / Accepted: 2 December 2022 / Published online: 14 December 2022
© The Author(s), under exclusive licence to Springer-Verlag GmbH Germany, part of Springer Nature 2022

Abstract
Transitional climate zone (TCZ) over East Asia is located between humid and arid regions, which is a highly sensitive and disaster-prone region especially under global climate change. Due to limited water resources, the atmospheric moisture availability has a dominant control on the precipitation variability. Hence, this study is motivated to reveal the key teleconnection patterns and associated moisture processes that govern the interannual variability of the summer precipitation over TCZ. In order to better diagnose moisture budget, the Lagrangian particle dispersion model FLEXPART is employed for quantifying contribution from moisture sources. Above all, the observational analysis highlights two critical modes, one is Eurasian teleconnection (EU) and the other is Circumglobal Teleconnection (CGT). As regards EU pattern, positive EU phase corresponds to ample precipitation in TCZ. In the presence of positive phase, it underlines a "+-+-" pattern of geopotential height anomalies stretching from western Europe to Mongolia plateau. In the context, the cyclonic flow and low pressure over Mongolia plateau act to enhance moisture flux from the west and the south and to prompt upward motions. Further moisture diagnoses illuminate largest increase of moisture uptake in monsoon dominated region, followed by the westerlies dominated region. However, the eventual contribution of summer monsoon is a little bit less than that of westerlies, due to the grand loss en route. In addition, the local evaporation exerts little impact. CGT propagates along the mid-latitude westerly jet, which is positively coupled with the precipitation in TCZ. Under the positive phase, there is an ascending motion over TCZ, which bears great resemblance to the EU case. However, unlike the result of moisture attribution in EU case, the southerly monsoon has the largest contribution followed by local effect, while the westerlies have little impact due to the cancellation of wetting and drying regimes along the pathway.

Keywords Transitional climate zone · Summer precipitation · Inter-annual variability · Lagrangian moisture tracking · Teleconnection · Mechanism

1 Introduction

Transitional climate zone (TCZ) over East Asia features a fragile ecosystem, violent climate oscillations, along with significant aridification with the pace of global warming (Ou and Qian 2006; Dai 2012; Huang et al. 2012a, b, 2020; Lu and Jia 2013; Chen et al. 2018; Piao et al. 2022). There have been large efforts from the scientific community devoting toward a better understanding of its interannual and interdecadal variability, especially for its wet-dry condition

✉ Lin Wang
linwang@mail.iap.ac.cn; wang_lin@mail.iap.ac.cn

✉ Gang Huang
hg@mail.iap.ac.cn

[1] CAS Key Laboratory of Regional Climate-Environment for Temperate East Asia, Institute of Atmospheric Physics, Chinese Academy of Sciences, Beijing 100029, China

[2] Hangzhou Meteorological Bureau, Hangzhou 310051, China

[3] State Key Laboratory of Numerical Modeling for Atmospheric Sciences and Geophysical Fluid Dynamics, Institute of Atmospheric Physics, Chinese Academy of Sciences, Beijing 100029, China

[4] College of Earth and Planetary Sciences, University of Chinese Academy of Sciences, Beijing 100049, China

[5] Carbon Neutrality Research Center, Institute of Atmospheric Physics, Chinese Academy of Sciences, Beijing 100029, China

(Huang et al. 2012a, b; 2017, 2019; Wang et al. 2021). Several studies have emphasized that the crucial roles of sea surface temperature (SST) anomalies over tropic Pacific and North Atlantic in summer rainfall variation over TCZ via the anticyclone over Western North Pacific (Zhao et al. 2019, 2020). The anomalous cyclone/anticyclone near Mongolia, East Asia westerly jet (EAWJ), the middle-tropospheric East Asian trough, and the western Pacific subtropical high (WPSH) also exert major impacts on climate variation in North China (Wang and Li 2011; Huang et al. 2012a, b; Piao et al. 2017; Chen et al. 2019; Guan et al. 2019; Lin and Bueh 2022). Additionally, the fact that all of these climate systems are affected by teleconnection patterns shows how crucial teleconnection modes are to the climate of the TCZ. By weakening the East Asian summer monsoon and shifting the WPSH southward, the Silk Road pattern, the Pacific-Japan (PJ) pattern, and the Eurasian teleconnection (EU) pattern, for instance, were to blame for the catastrophic summer drought that hit North China and Northeast Asia in 2014 (Wang and He 2015). There are also evidences showing a connection between decadal change of summer precipitation in Northeast Asia in late 1990s and the circulation anomalies under the combined impacts of the Pacific decadal oscillation (PDO) and the Atlantic multidecadal oscillation (Piao et al. 2020, 2021).

Teleconnection refers to the phenomenon of the climate links between meteorological elements in geographically separated regions. Its propagation and maintenance are closely related to large scale persistent weather and climate anomalies, such as El Niño-Southern Oscillation (ENSO) phenomenon (Bjerknes 1969; Wang et al. 2017a, b), and the Madden Julian Oscillation (Madden and Julian 1971; Li et al. 2020). Aside from the examples mentioned above, three teleconnection patterns and their associated circulation anomalies have received most attentions since the current century, when it comes to summer climate variation in East Asia, which are EU teleconnection over Eurasia, Circumglobal teleconnection (CGT) along with mid-latitude westerly jet, and PJ teleconnection over East Asia (Wakabayashi and Kawamura 2004; Ding and Wang 2005; Ding et al. 2011; Kosaka et al. 2011; Liu et al. 2014; Kubota et al. 2015). For example, it has been proposed that the persistent droughts of North China during 1999–2000 are the consequence of the intensified Rossby wave train over Eurasia continent during summer (Jie et al. 2004). Zhang et al. (2018) also found that Arctic sea ice concentration from preceding spring to summer has a considerable impact on precipitation in northern Northeast China through circulation anomalies related to EU pattern. In addition, as the most prominent feature in the 200-hPa height field in interannual time scale, CGT also has significant influences on surface temperature and land precipitation in East Asia (Ding et al. 2011). Wang et al. (2017a, b) demonstrated that Silk Road teleconnection, which also has been considered as the regional manifestation of CGT pattern (Ding and Wang 2005), was also substantially connected with precipitation in northern China based on observational data. Different from the first two teleconnections which both are zonal Rossby wave train, PJ pattern exhibits meridional dipole structure of circulations in the lower troposphere and precipitation anomalies in the western Pacific and mid-latitude. PJ pattern is also used to represent the intensity of the East Asian summer monsoon and shows close connection with preceding ENSO (Huang 2004; Kubota et al. 2015).

Based on observation data, the characteristics of wet-dry condition variation of summer over TCZ in the past 60 years are dominated by the interannual oscillation mainly driven by precipitation (Wang et al. 2021). Sufficient water vapor and ascending motion are essential conditions for precipitation. The moisture source for precipitation is composed of water vapor contained in the atmosphere over the region, water vapor transport from outside and local evaporation. Located in the semi-arid areas, water resource of TCZ is limited compared to humid area. When describing mechanisms of water vapor budget and precipitation anomalies, most previous studies focus on water vapor transport field or water vapor equation based on Eulerian method, but it fails to provide information on the geographical sources of the moisture (Chou et al. 2009; Seager et al. 2010; Xu et al. 2015; Zhou et al. 2017). However, lagrangian diagnosis with the help of lagrangian particle dispersion models (LPDMs), such as the Hybrid Single-Particle Lagrangian model (HYSPLIT) and the FLEXible PARTicle model (FLEXPART), has been wildly used and proved reliable in the hydrologic cycle research (Bin et al. 2013; Hao et al. 2014; Sun and Wang 2014, 2015; Salih et al. 2015). It shows its advantages over Eulerian method in source-sink relationship with quantitative results by tracking air parcels moving with the wind field including their three-dimensional spatial position and moisture content. According to the results derived from FLEXPART output, our previous study suggested that main moisture source for summer precipitation in TCZ comes from external water vapor transported by mid-latitude westerlies and the summer monsoon circulations, which together contribute about two-thirds of the water vapor (Wang et al. 2022). In fact, this study is built on the previous one. Combined with ascending motion analysis, precipitation moisture supply is investigated with Lagrangian method in this study to get a better understanding of the physical mechanisms of the interannual variability of summer precipitation of TCZ.

The rest of the paper is organized as follows: data and methodology are described in Sect. 2. Section 3 identifies the major teleconnection patterns and their influencing mechanisms to the interannual variation of summer precipitation in TCZ. Finally, a summary and discussion are given in Sect. 4.

2 Data and method

2.1 Data and model simulation

The trajectory data used in this study is the 32-year simulations of FLEXPART_10.4v for summers (5.21–8.31) of 1979–2010. The model was run forward in time with one million particles released globally at beginning of the simulations using "domain fill" mode. The National Centers for Environmental Prediction–Climate Forecast System Reanalysis (NCEP–CFSR) 6-hourly forecast dataset (Saha et al. 2010) from 1979 to 2010 is employed as model driving data, including land cover, temperature, relative humidity, and three-dimensional winds at 42 levels with a horizontal resolution of 0.5° × 0.5°. The model output is saved at 6-h intervals.

The observation daily precipitation dataset during summer (Jun–Aug) from 1979–2010 is retrieved from National Meteorological Information Center, with a spatial resolution of 0.5° × 0.5°, which originates from observations of more than 2000 meteorological stations in China (Xu et al. 2019). The 6-h Reanalysis datasets during the same period including three-dimensional wind, geopotential height, and surface pressure applied in this study are the Japanese 55-year Reanalysis (JRA-55) (Kobayashi et al. 2015; Harada et al. 2016), with a resolution of 1.25° × 1.25°.

2.2 Lagrangian diagnosis and three moisture sources for summer precipitation of TCZ

In this study, Lagrangian diagnosis is introduced to quantify the moisture contribution from different sources and dominant systems as well as moisture release/uptake situation during transportation. For an air particle, the net change rate of the water vapor content can be expressed as follows (Stohl and James 2004):

$$e - p = m\frac{\mathrm{d}q}{\mathrm{d}t} \tag{1}$$

where e and p are the rates of moisture uptake and release along the trajectory, respectively, and m and q are the air mass and specific humidity. dq/dt is the change of specific humidity with time. Here dq/dt = q(T)-q(T-6 h), since the model output is saved at 6-h time intervals. However, a threshold of 0.2 g/kg/6 h instead of 0 is used as the criterion of moisture uptake (dq/dt > 0.2 g/kg/6 h) or release (dq/dt < − 0.2 g/kg/6 h) to avoid errors from numerical noise (James et al. 2004; Sodemann et al. 2008; Huang and Cui 2015).

The surface freshwater flux (E-P) and moisture content (W) over an area A can be given as

$$E - P = \frac{\sum_{k=1}^{k=K}(e-p)}{A} = \frac{\sum_{k=1}^{k=K} m\frac{dq}{dt}}{A} \tag{2}$$

$$W = \frac{\sum_{k=1}^{k=K} mq}{A} \tag{3}$$

where K is the total number of particles in the atmospheric column over A. It can be inferred from the Eqs. (2) and (3) that the E-P and W is not only related to the moisture of the individual target particle, but also depend on the number of target parcels contained in the column over domain A. The moisture content (W) reflects the total water vapor mass density of all target particles over domain A, while the E-P reflect the change of the total water vapor mass. The average residence time period of water vapor in the atmosphere is about 10 days (Numaguti 1999). Therefore, the first 10 days before the arrival of the target air mass that release moisture in the TCZ from June 1st to August 31st are selected as the target trajectories. The E-P diagnoses of target back-trajectories can be used to determinate moisture sources of the target region, when positive (negative) E-P indicates a source (sink) region (James et al. 2004; Sodemann et al. 2008; Sun and Wang 2014, 2015). As shown in Fig. 1, the moisture supply for summer precipitation of TCZ mainly come from three parts: most Eurasian continent to the north and west of TCZ where the belt of mid-westerlies is the dominant system, summer monsoon system controlled regions including central-eastern China, northwest Pacific Ocean and north Indian Ocean, and local evaporation. According to dominant system of each moisture source regions, quantitative contribution of these three systems has been figured out in our previous study (Wang et al. 2022). The calculation procedure of quantification of moisture contribution from source regions is based on Lagrangian diagnosis and can be summarized as follows. First, find out particles which had moisture release over TCZ, and accumulate every moisture release of all selected particles as the total moisture release

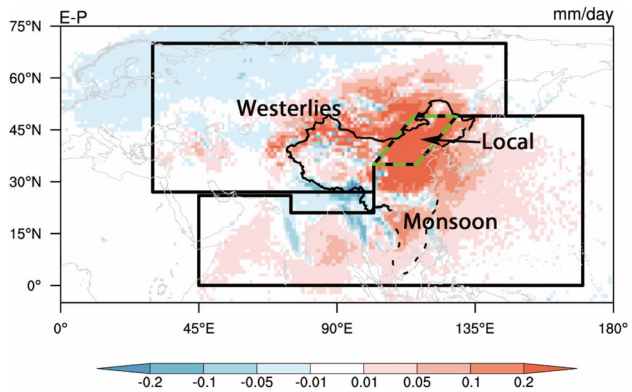

Fig. 1 Mean E-P of target-bound air parcels in 1–10 days (−240~− 6 h) before releasing moisture over TCZ and three dominated systems in moisture source regions of TCZ in summer of 1979–2010 (Wang et al. 2022). The three systems include monsoon, westerlies and local evaporation. The green dashed parallelogram encloses the TCZ domain

(Rtotal, unit: kg). Even though Rtotal can't be exactly equivalent to lagrangian precipitation, its variability can represent variation of simulated precipitation to some extent. Second, for each examined moisture source regions, pick out target particles which had moisture uptake over the region from the particles obtained in the previous step. Third, for every target particle, track the moisture content from the source region so the moisture contribution from examined source region can be evaluate and accumulated every time when the moisture release happened in TCZ. At last, accumulate moisture contribution of all selected particles as the moisture contribution of examined source region (CON, unit: kg), and then define the ratio of CON to Rtotal as relative moisture contribution (RCON, unit: %). More details and the flow chart are available in our previous work (Wang et al. 2022).

2.3 Takaya–Nakamura (T-N) wave activity flux

The Takaya–Nakamura (T-N) wave activity flux (TNF) was used to diagnose the Rossby wave and the direction of wave energy propagation. This method was developed by Takaya and Nakamura (2001) and the horizontal wave activity is mathematically written as:

$$\mathbf{F} = \frac{p\cos\phi}{2|\mathbf{U}|}\begin{pmatrix} \left(\frac{U}{a^2\cos^2\phi}\left(\psi_\lambda'^2 - \psi'\psi'_{\lambda\lambda}\right) + \frac{V}{a^2\cos\phi}\left(\psi'_\lambda\psi'_\phi - \psi'\psi'_{\lambda\phi}\right)\right) \\ \frac{U}{a^2\cos\phi}\left(\psi'_\lambda\psi'_\phi - \psi'\psi'_{\lambda\phi}\right) + \frac{V}{a^2}\left(\psi_\phi'^2 - \psi'\psi'_{\phi\phi}\right) \end{pmatrix} \tag{4}$$

where p = pressure/1000 hPa, $\mathbf{U}$ = (U, V), ψ' denote the nomalized pressure, basic wind velocity, and perturbed geostrophic stream function, respectively. The subscript represents the partial derivative. λ, ϕ, a stand for latitude, longitude, and the earth's radius, respectively. Here, the basic field, in which atmospheric waves propagate, is assumed to be summer mean (JJA) from 1979 to 2010.

2.4 Statistical analysis

Statistical methods commonly used in meteorological research, including empirical orthogonal functions (EOF) analysis, composite analysis, Pearson correlation analysis, and linear regression analysis have been applied in this paper. In addition, since this work fucuses on the interannual variation of wet/dry condition of TCZ, interannual component of all variables in this study has been extracted via a 9-yr high pass filter using Fourier analysis technique with linear trend being removed first.

Given that there are two major teleconnection patterns were identified, we also utilized partial correlation analysis as the supplement to the credibility of the results. The partial correlation coefficient $r_{AB|C}$ between A and B, which is statistically independent from time series C, can be expressed as (Lin and Bueh 2022):

$$r_{AB|C} = \frac{r_{AB} - r_{AC}r_{BC}}{\sqrt{1 - r_{AC}^2}\sqrt{1 - r_{BC}^2}} \tag{5}$$

where r_{AB}, r_{AC}, r_{BC} denote the simple correlation coefficients between A and B, A and C, and B and C, respectively.

3 Results

3.1 Identification of main teleconnection patterns with observed data

This work takes advantage of the Lagrangian tracking algorithm based on FLEXPLART model to quantify the humidity contribution to moisture budget over TCZ along the backward trajectories, which is superior to Eulerian diagnosis. As we depend on the simulated data, the validation of lagrangian results against observed summer (Jun-Aug) precipitation in TCZ becomes a critical prerequisite. Figure 2 is depicted to compare the regional averaged anomalies between observed summer rainfall and total moisture release (Rtotal) over the TCZ, as well as their corresponding interannual components. Contrasting the raw sequence, the interannual fluctuation of total water vapor release over the TCZ in summer appears to be more concordant with observed precipitation variation. The Pearson correlation coefficient of the two interannual components is amounting to 0.73, whereas that of the raw series is merely 0.59. Therefore, the tight interannual co-variability between total water vapor release and observed precipitation justify that the Lagrange simulated results can accurately capture the interannual oscillation of summer precipitation in the TCZ.

In order to shed light on the key teleconnection modes affecting summer precipitation in the TCZ, regression analyses of geopotential height and horizontal winds on multiple standard isobaric levels are performed on both observation

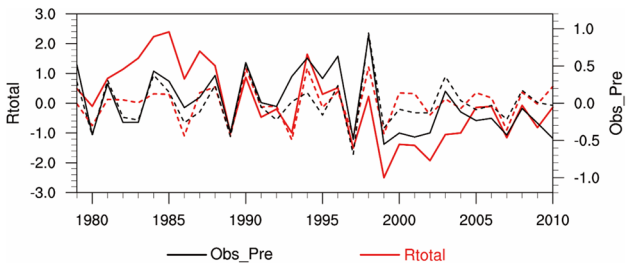

Fig. 2 Anomalies of observed precipitation (black solid line, units: mm/day) and total moisture release over TCZ (red solid line, units: 10^{14} kg) in summer during 1979–2010. Dashed lines are corresponding interannual components

precipitation and total moisture release separately, as shown in Fig. 3. The most striking feature of the regression map is the alternation of positive and negative geopotential height anomalies over Eurasia, which exhibits four anomaly centers at all tropospheric levels over the Mediterranean region, the Scandinavian Peninsula, the Ural Mountains region, and Mongolia plateau (Fig. 3a, c, e). This equivalent barotropic structures agree well with the well-known Eurasian teleconnection pattern (EU) which have been investigated by previous research (Iwao and Takahashi 2006; Zhang et al. 2018; Ming et al. 2019). Another distinguishing characteristic reflects a sequence of pressure anomalies propagating along the Silk Road in the upper troposphere (Fig. 3e), comparable to the global wave train pattern of circumglobal teleconnection (Ding and Wang 2005; Huang et al. 2011), with anomalous quasi-barotropic high pressure over the Sea of Japan (Enomoto et al. 2003). It concludes that summer precipitation interannual variations in the TCZ is mainly promoted by variation of atmospheric circulation associated with the EU and CGT patterns. Similar results can be obtained from the regression maps of moisture total release (Fig. 3b, d, f), with relative weaker teleconnection anomalies in the

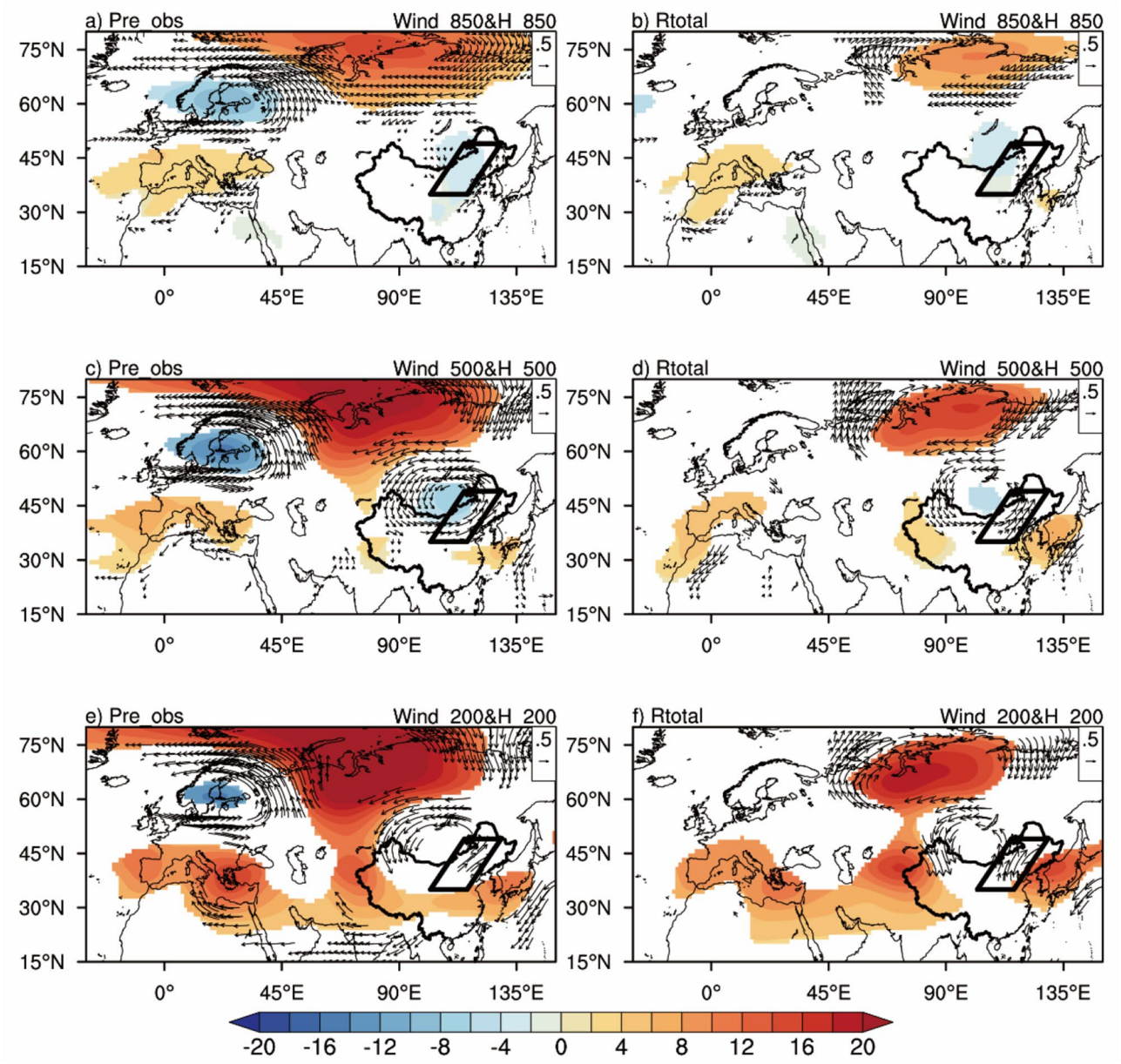

Fig. 3 The regression patterns of the geopotential height (shadings, unit: gpm) and horizontal wind (vectors, unit: m s^{-1}) at 850 hPa, 500 hPa and 200 hPa in summer during 1979–2010 onto observed precipitation (**a**, **c**, **e**) and total moisture released (**b**, **d**, **f**), respectively. Only values significant at the 95% confidence level are drawn

upstream region over Europe compared to observations. However, regrresion results without any filtering preprocesses based on significant test, shows that circulation anomalies related to Rtotal and observed precipitation bear a fairly close resemblance (Figure not shown). One of the reasons caused the differences between model results and observation may be the assumption that all moisture decrease is due to precipitation and that precipitation falls immediately (James et al. 2004; Sodemann et al. 2008). And the threshold of specific humidity change of 0.2 g/kg per 6 h used to determine moisture uptake or release (James et al. 2004; Sodemann et al. 2008; Huang and Cui 2015) can't fully reflect the actual situation. This discrepancy between model results and observation also has been discussed in our previous work (Wang et al. 2022). However, this slight difference is not enough to affect the fidelity of using Lagrangian simulation to gain deep insights into how the teleconnections influence the moisture transport and budget over TCZ. Therefore, the following investigation deal with the water vapor response and dynamic process driven by EU and GCT.

3.2 Eurasian teleconnection pattern

The Eurasian teleconnection, first identified by Wallace and Gutzler (1981), features a mid-tropospheric, west–east-oriented wave train over Eurasia, which usually has more than three atmospheric centers of action and has a variety of structures with different influencing mechanisms. EU pattern is generally defined by anomalies in atmospheric general circulation at 500 hPa over Eurasian (Wakabayashi and Kawamura 2004; Ming et al. 2019). In this study, EOF analysis is used to determine the primary EU teleconnection patterns with geopotential height anomalies at 500 hPa across the mid-high latitude region of the Eurasian continent (60° W–160° E, 30° N–80° N) during summer from 1979 to 2010 (Figure not shown). The first two modes account for 24.9% and 14.8% of the total variance, respectively, and can be well isolated from other modes based on the criteria proposed by North et al. (1982). The first mode is mainly characterized by the "-+" dipole structure covering Western Europe and the North Pacific Ocean, with only a weak negative height anomaly over TCZ. Thus, the first EOF mode is not our concern. Nevertheless, the second EOF mode is strongly consistent with the regressed circulation anomalies at 500 hPa related to TCZ summer precipitation (Fig. 3c). Subsequently, the corresponding time coefficient of the second mode is used in this study as EU index (EUI) to further investigate the impact of EU pattern on summer precipitation over TCZ. Figure 4 depicts EU pattern related circulation anomalies at 500 hPa and corresponding wave activity flux based on regressed geopotential height. With strenuous wave activity fluxes in the northeast-southeast direction over Eurasia, this pronounced teleconnection wave train results

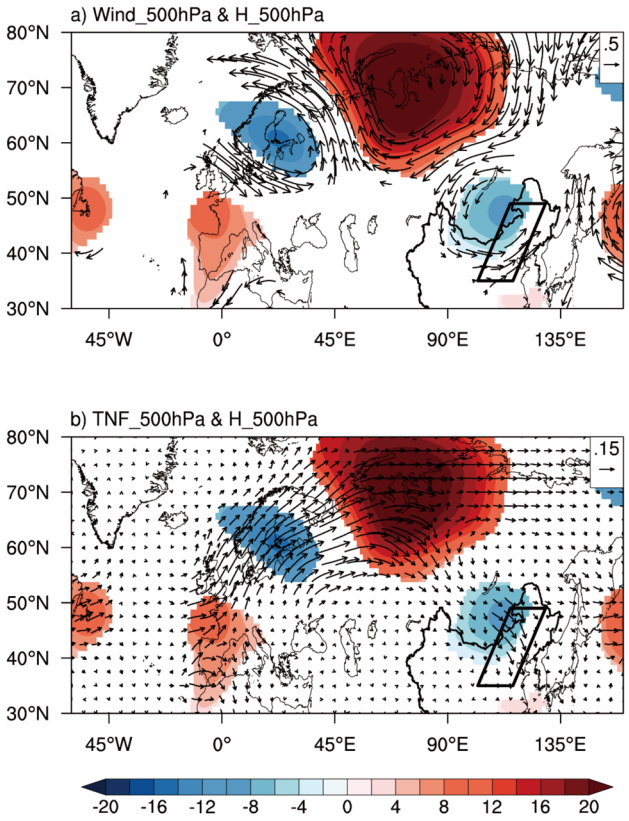

Fig. 4 **a** The regression map of horizontal wind (a, vector, unit: m s^{-1}) and geopotential height (shading, unit: gpm) at 500 hPa in summer (JJA) during 1979–2010 onto standardized interannual component of EUI, as well as the corresponding horizontal wave activity flux (**b**, vector units:$m^{-2}s^{-1}$). Horizontal wind and the geopotential height are significant at the 95% confidence level

in a series of "anticyclone-cyclone-anticyclone-cyclone" wind field anomalies as well as "+-+-" geopotential height anomalies. It emanates from the Mediterranean region and propagates across the Scandinavian Peninsula and the Ural Mountains and finally terminates in the Mongolian plateau. In the context, the cyclonic flows emerged over Mongolia boosts westerly and southwesterly winds in the south of TCZ and the anomalous low pressure leads to convergence of horizonal wind. The linear correlation between EUI and observation precipitation (Rtotal) reaches 0.79 (0.56), which exceeds the significance test of 95% confidence level and further proved their close connections.

In what follows, composite analysis is carried out for better understanding the dynamic and moisture processes. To this end, a positive and negative EU phase is defined using 0.75 standard deviation of the interannual component of EUI as a threshold. This criterion yields seven years for positive and negative cases as listed in Table 1. The composite positive (negative) EU pattern, labeled as EU_pos (EU_neg), is constructed from the average of all

Table 1 List of EU_pos, EU_neg years

	year
EU_pos	1979/1981/1984/1990/1994/1998/2009
EU_neg	1980/1991/1992/1995/1997/2002/2007

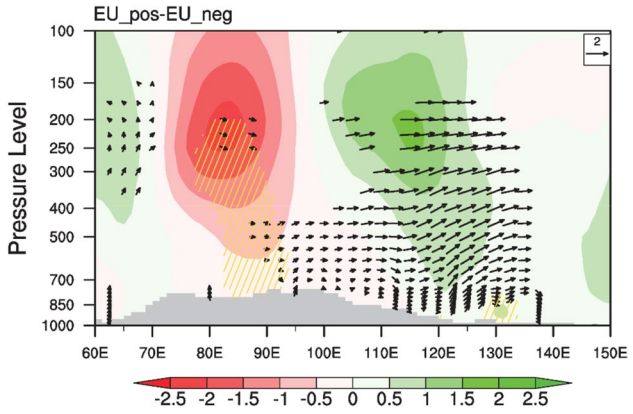

Fig. 5 Composite differences between years of EU_pos and EU_neg of the meridional wind (shadings, unit: m s^{-1}) and the zonal-vertical cell of circulation (vector, the vertical velocity is amplified by 100 times) averaged along 35°–49° N. The vectors statistically significant at the 95% confidence level are shown. Yellow hatches indicate the difference in meridional wind is statistically significant at the 95% confidence level

positive (negative) EU years. Vertical cross section of composite circulation anomalies o between EU_pos and EU_neg is shown in Fig. 5. The cyclone over Mongolia (80°–130° E) tends to be maintained from the lower to the upper troposphere, manifesting an equivalent barotropic structure. This cyclonic anomaly strengthened westerly wind anomalies throughout the troposphere over TCZ. To the south of TCZ, substantial southerly wind anomalies are observed at lower level of the troposphere, which is beneficial for summer monsoon moisture transport. What's more, it is hard to neglect the ascending motion anomalies over TCZ (102°–129° E), except the sinking motion anomalies in lower troposphere among 100°–115° E. The center longitude of the cyclone over Mongolia is near 100° E, which making TCZ locate in front of the trough. Therefore, we resort to the linearized geostrophic omega equation (Kosaka and Nakamura 2010; Hu et al. 2017; Xu et al. 2022) without considering diabatic processes to get a better understanding of dynamic mechanism of the vertical motion anomalies:

$$\omega' = -\left(\nabla^2 + \frac{f}{\sigma_s}\frac{\partial^2}{\partial p^2}\right)^{-1}\frac{f}{\sigma_s}\frac{\partial}{\partial p}\underbrace{\left(-\bar{V}_g\cdot\nabla\zeta_g' - V_g'\cdot\nabla(\bar{\zeta}_g+f)\right)}_{\textit{vordicity advection}}$$
$$-\left(\nabla^2 + \frac{f}{\sigma_s}\frac{\partial^2}{\partial p^2}\right)^{-1}\frac{R}{\sigma_s p}\nabla^2\underbrace{\left(-\bar{V}_g\cdot\nabla T' - V_g'\cdot\nabla\bar{T}\right)}_{\textit{temperature advection}} \quad (6)$$

Where f, V_g and ζ_g donate Coriolis parameter, geostrophic horizontal wind vector, the vertical component of geostrophic relative vorticity, respectively. σ_s is the static stability can be calculated by $\sigma_s = \frac{R}{p}(\frac{R\bar{T}}{c_p p} - \frac{\partial\bar{T}}{\partial p})$. $R = 287\,\mathrm{J kg^{-1} K^{-1}}$ and $c_p = 1004\,\mathrm{J kg^{-1} K^{-1}}$ are the gas constant for dry air and the specific heat of dry air at constant pressure, respectively. The overbar denotes the climatological mean, and the prime denotes the differences between EU_pos and EU_neg years. The two terms on the right-hand side of Eq. (6) are stand for abnormal ascending motion caused by the vertical distribution of vorticity advection and the horizontal temperature advection. The conclusions can be drawn that increasing horizontal vorticity advection with height and warm horizontal advection can both lead to the enhancement of ascending motion. Figure 6 shows the horizontal vorticity advection and the temperature advection over TCZ. It is noticeable that strong positive vorticity advection anomalies in the upper troposphere over TCZ are consistent with the enhanced ascending motion below them. There is warm temperature advection in the middle and upper troposphere, enhancing the upward motion there. However, both of them are not quite enough to the ascending motion center in the lower troposphere over east part of TCZ (122–125° E), indicating the possible exsistence of other influencing factors, such as the diabatic heating caused by enhanced precipitation.In parallel to dynamic assessment, the following analyses are centered on moisture supply of summer precipitation in the TCZ and the changes during its transport under different EU modes using the Lagrangian diagnostic results, given that the occurrence of precipitation requires an adequate supply of water vapor especially over TCZ. The E-P diagnosis of the target trajectories are useful for determining water vapor exchange between land/ocean and atmosphere during the transport. Positive values of E-P indicate that the air mass tends to gain humidity when it is over a certain region, while moisture release is dominant when E-P < 0. Meanwhile, moisture content reflects the wetness of the target particles, whose variation shows the overall change of water vapor content in the whole region more intuitively during transportation. The spatial distribution of E-P and moisture content along with moisture content are shown in Fig. 7. In the positive phase of EU, on the one hand, bounded air parcels tend to earn more water vapor when passing the westerlies upstream areas of the TCZ,

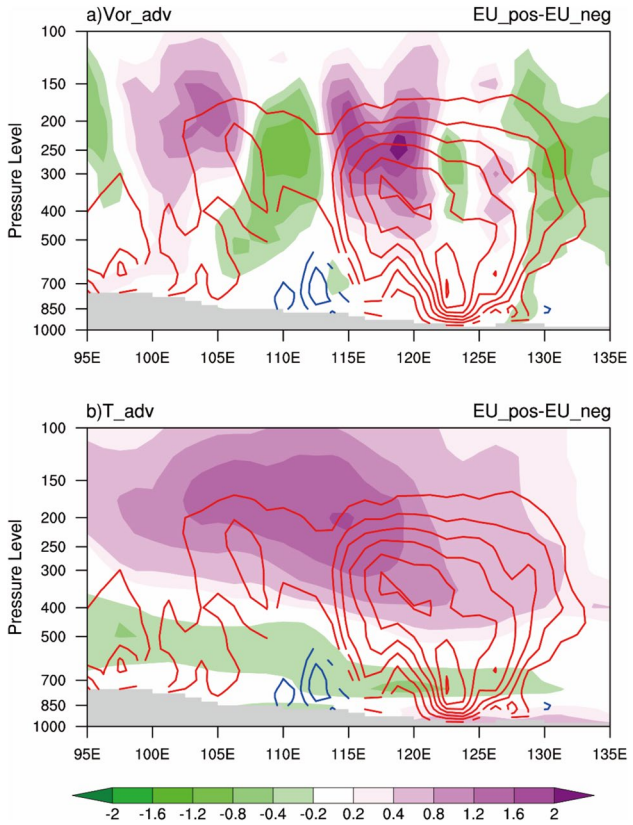

Fig. 6 **a** Latitude–height cross section of the horizontal vorticity advection anomalies (shading, unit:10^{-11} s^{-2}) and vertical pressure velocity (contour; CI = 0.002 hPa s^{-1}; ascending motion with negative values are contoured by red lines, downdraft with positive values are blue lines) averaged between 35° and 49° N and between years of EU_pos and EU_neg. **b** As in (**a**), but for the anomalies of horizontal temperature advection (unit:10^{-5} K s^{-1})

especially in the northern fringe of Tibetan Plateau and the Western Siberian Plain regions, which helps to raise their moisture content (Fig. 7a–b). On the other hand, moisture content of air parcels stemming from the Indian Ocean, the western Pacific, and southeastern China are also increases, and is replenished when passing the Yangtze River and Huaihe River basins. As a consequence, much stronger moisture release is noted in the target TCZ region, leading to ample precipitation there. Compared to EU positive phase, we further point out a generally opposite pattern typically associated with EU negative phase, which will not be interpreted here.

The above analysis provides a broad-scale spatial perspective. Then, the discrete grid-scale information can be bundled into three large blocks according to the dominant climatic systems, as refer back to Fig. 1. Figure 8 shows the correlation and regression analysis of the interannual components of the water vapor contributions from summer monsoon, the mid-latitude westerly winds and local evaporation with the EUI. Both summer monsoon systems and mid-latitude westerlies show significant positive correlations with EUI with correlation coefficients of 0.36 and 0.47 with the corresponding regression coefficients are 1.69×10^{13} kg and 1.43×10^{13} kg, respectively. However, moisture contribution from local evaporation exhibits no significant relation with EUI, as reflected by the trivial correlation coefficients of 0.21. As the moisture uptake over a source region (Uptake) equals to the sum of three parts including moisture loss en route (Loss), unreleased moisture over the target area (Unreleased), and moisture contribution to the precipitation (Contribution) (Sun and Wang 2014), our concerning 'Contribution' term can be mathematically written as Contribution = Uptake-Loss-Unreleased. We next decompose the 'Contribution' change into these three components. In this way, the differences in the average moisture contribution between EU_pos and EU_neg driven by, as well as moisture uptake, en-route loss and unreleased are shown in Fig. 9. Compared with the negative phase of EU, the water vapor absorbed over source regions for all the three systems increases in the EU positive phase year, with the largest increase noticed in the monsoon dominated region (7.59×10^{14} kg), followed by the westerly dominated region (7.44×10^{14} kg). Compared to the enormous moisture uptake enhancements over these two regions, the increasements of the actual water vapor contributions to the summer precipitation over TCZ are rather small with 0.63×10^{14} kg from monsoon system and 0.60×10^{14} kg from the mid-latitude westerlies, due to the large loss of water vapor en route—both over 6.0×10^{14} kg. The increase in water vapor absorbed over the TCZ makes marginal difference (0.66×10^{14} kg) between the opposing phase of EU, so that its moisture change makes the least contribution increase (0.25×10^{14} kg) of three major moisture source.

As a concluding remark, the positive phase of EU teleconnection offers favorable circulation condition, which not only induces upward motion over TCZ, but also brings extra moisture supplies from monsoon systems and westerlies.

3.3 Circumglobal teleconnection pattern

Enomoto et al. (2003) offered that the Bonin high, the equivalent barotropic warm anticyclone over the Sea of Japan in summer, is the result of the propagation of stationary Rossby waves along the Asian jet in the upper troposphere (Silk Road pattern). Subsequently, Ding and Wang (2005) proposed that teleconnections positioned within a waveguide that is associated with the westerly jet stream, such as the ISM–EASM teleconnection, the Silk Road, and the Tokyo–Chicago express, are regional manifestations of CGT pattern in boreal summer. In order to explore the influence of CGT on the interannual variation of summer precipitation in TCZ, the definition initiated by Ding and Wang (2005) is adopted in this study. The circumglobal teleconnection

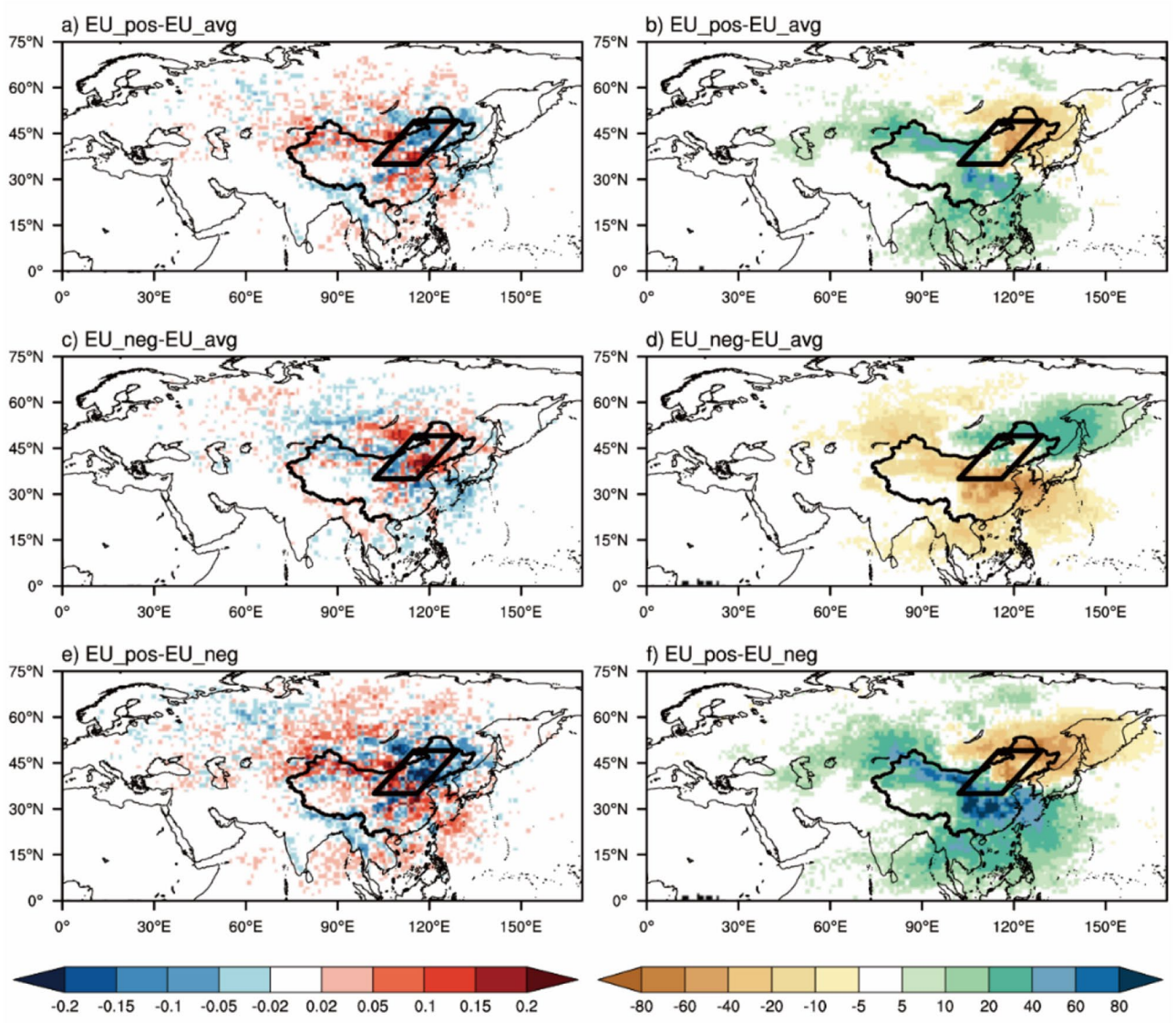

Fig. 7 Composites of Mean E-P (**a**, **c**, **d**, unit: mm day^{-1}) and moisture content (**b**, **d**, **f**, unit: kg m^{-2}) anomalies of target-bound air parcels averaged over 10 days (from −240 to − 6 h) before reaching TCZ (0 h) in EU_pos years, EU_neg years and their differences. EU_avg refers to the climatological results

index (CGTI) is defined as the average geopotential height anomalies of 200 hPa over the western-central Asian domain (35°–40° N, 60°–70° E). Above all, the interannual component of CGTI is positively correlated with the observed summer precipitation in the TCZ and the total water vapor release from the Lagrangian simulation of the air mass over the TCZ, with correlation coefficients being 0.38 and 0.46 respectively. Figure 10 shows regressed anomalies of geopotential height on interannual variability of CGTI, showing that there are multiple geopotential height anomalies centers at mid-latitudes, which are mainly manifested as positive pressure anomaly centers in west-central Asia and East Asia (Enomoto et al. 2003). Even though CGT and EU pattern are both important teleconnections in the northern hemisphere (Fig. 3), the linear correlation analysis shows no significant correlation (r = 0.21) between the two indices in interannual scale. Therefore, the roles of EU pattern and CGT are discussed separately in this study. The partial correlation analysis is also applied in order to better eliminate the impact from EU pattern, which showed little differences compared to the simple correlation (Table 2), which further verifies the rationality to separately study the influence mechanism of the two patterns.

Next, similar composite approaches as done in Sect. 3.2 are applied to examine the main mechanism of how atmospheric circulations linking CGT and TCZ summer rainfall.

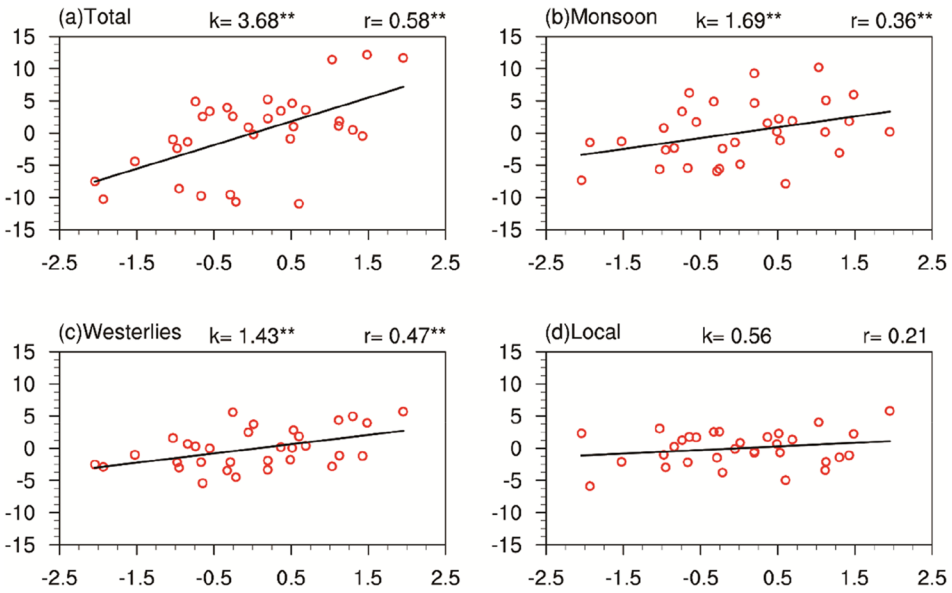

Fig. 8 Scatter plot of standardized interannual component of EUI (X-axis) versus moisture total release (**a**) and moisture contributions (Y-axis, unit: 10^{13} kg) from different systems including summer monsoon circulations (**b**), mid-latitude westerlies (**c**) and local evaporation (**d**) with linear regression line superimposed (black line). The values of k and r are the regression and correlation coefficients. */** indicates coefficients statistically significant at the 90%/95% confidence level

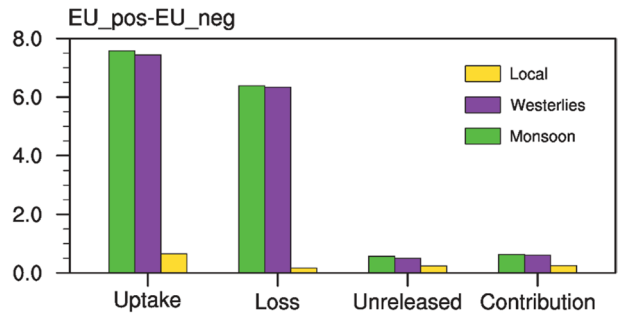

Fig. 9 The differences in the average absolute contribution (Contribution) between years of EU_pos and EU_neg driven by summer monsoon (green), the mid-latitude westerly winds (purple) and local evaporation (yellow), as well as the total moisture uptake (Uptake), en-route loss (Loss) and unreleased water vapor (Unreleased), unit: 10^{14} kg

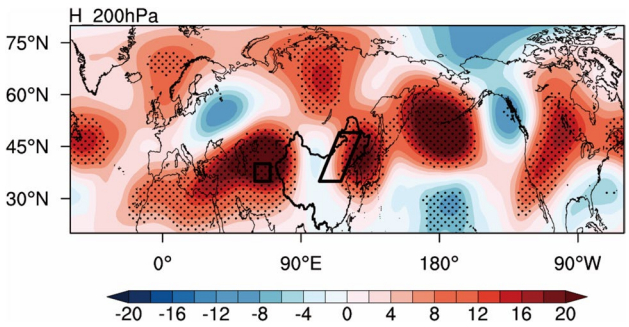

Fig. 10 The regression patterns of the geopotential height (contour, unit: gpm) at 200 hPa in summer (JJA) during 1979–2010 onto standardized interannual component of CGTI, respectively. Dots indicate significant at the 95% confidence level

Table 2 Simple correlation coefficients and Partial correlation coefficients of EUI/CGTI and moisture total release and moisture contributions from regions dominated by summer monsoon circulations, westerlies and local evaporation

Index	System	Simple linear correlation	Partial correlation
EU	Rtotal	0.58**	0.52**
	Monsoon	0.36**	0.33*
	Westerlies	0.47**	0.38**
	Local	0.21	0.18
CGT	Rtotal	0.44**	0.43**
	Monsoon	0.45**	0.39**
	Westerlies	− 0.06	− 0.05
	Local	0.32*	0.27

*/**Indicates coefficients statistically significant at the 90%/95% confidence level

Table 3 List of CGT_pos and CGT_neg years

	Year
CGT_pos	1980/1984/1990/1994/2001/2003/2006/2008
CGT_neg	1981/1982/1987/1992/1993/1999/2004/2009

CGT positive and negative phase years are extracted by using 0.75 standard deviation (Table 3), and 8 years in each phase were selected as listed in Table 3. The composite differences in the meridional wind and the zonal-vertical circulation between CGT_pos and CGT_neg is illustrated in Fig. 11. At first glance, ascending motion above TCZ is noted in

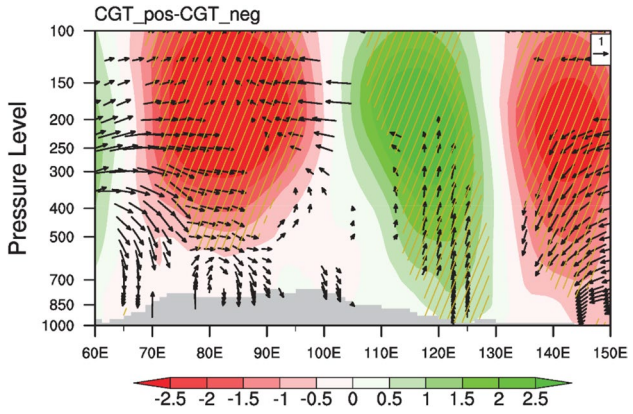

Fig. 11 Same as Fig. 5, but for CGTI

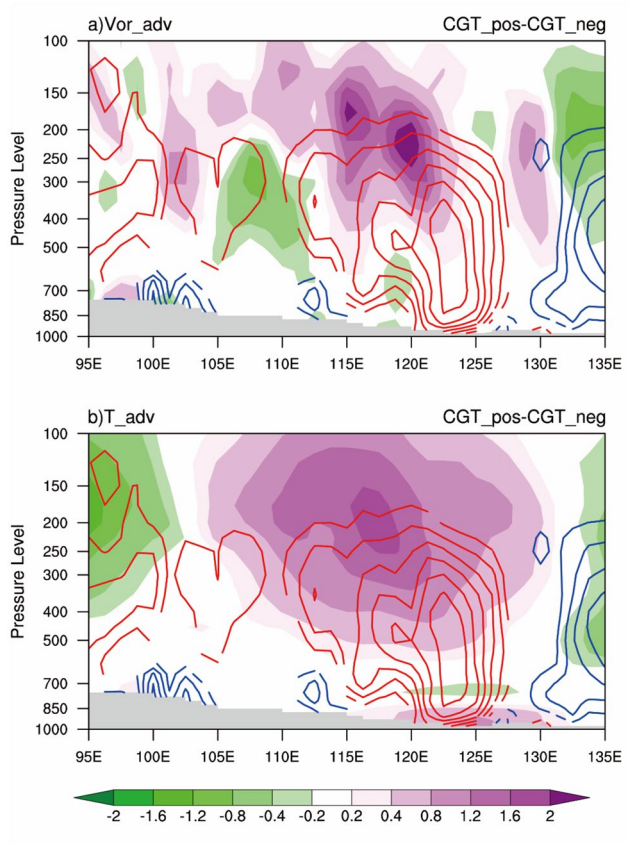

Fig. 12 Same as Fig. 6, but for CGTI

positive phase years of CGT, which bears great resemblance to EU case. It can be concluded based on Fig. 12 that the strong ascending motion can be attributed to the increase of horizontal vertical vorticity advection with height and warm temperature both in lower troposphere (below 850 hPa) and higher level (above 700 hPa). However, the key discrepancy relative to EU case is that in the case of positive CGT the southerly winds play a major role that overwhelms the whole troposphere, whereas the westerly winds is not as such pronounced. In addition, the consistency of the circulation configuration on the east and west sides of 130ºE at the different altitudes confirms an equivalent barotropic structure, in line with previous studies (Enomoto et al. 2003, Wang and He 2015).

Apart from dynamic investigation, the attribution of moisture changes during the transportation will be discussed as follows. The spatial distribution of lagrangian E-P analysis and water vapor content of target trajectories are displayed in Fig. 13. Remember in the EU case, the moisture stemming from subtropical ocean undergoes uniform gain en-route (Fig. 7e–f), irrespective of the pathway. However, this is not the case for CGT-related response. The positive phase of CGT gives rise to a positive E-P anomaly in the western Pacific at lower latitudes (south of 30ºN), leading to increased water vapor absorbed by the target air parcel over the source region. But over the Yellow Sea of China, the moisture content anomaly is negative with $E\text{-}P < 0$ (Fig. 13e–f), which means that the particles passing over this area tend to gain less moisture in CGT_pos years. Even so, the overall effect of southerly monsoon is to make more rainfall over the target TCZ (Figs. 14 and 15). An integrated view puts forward that moisture increase over East China sea is much larger than that of decrease over the East China. Next, we turn to the air parcels travelling along with westerlies. It can be seen that moisture content experiences wetting regime in the Central Asia but drying regime in Mongolia, and such fluctuations tend to cancel out each other. This makes the westerlies having little net effect on precipitation over TCZ, which will be further quantified.

In subsequent, evaluation of moisture contributions from three major climatic systems in response to CGT will be explored. Figure 14 shows the results of correlation and regression analysis of the interannual components of the water vapor contributions from summer monsoon, the mid-latitude westerly winds and local evaporation and with the GCTI. Above all, it is found a significant positive correlation between CGTI and water vapor contribution from local evaporation and summer monsoon circulation over TCZ, with the correlation coefficients of 0.32 and 0.45, respectively (Fig. 14b, d). Based on the fitting lines, the monsoon moisture contribution is most sensitive to CGT index with regression coefficient being 2.1×10^{13} kg, which is about three times more than that of local contribution whose regression slope is 0.85×10^{13} kg. Apart from monsoon and local effects, the water vapor supply conveyed by westerlies seems to be decoupled from the CGT index, because both the correlation coefficient and regression coefficient are not statistically significant (Fig. 14c).

This confirms the previous assertion that the positive and negative anomalies along the westerly pathway would cancel out. Next, the three essential factors (uptake, loss, unreleased)

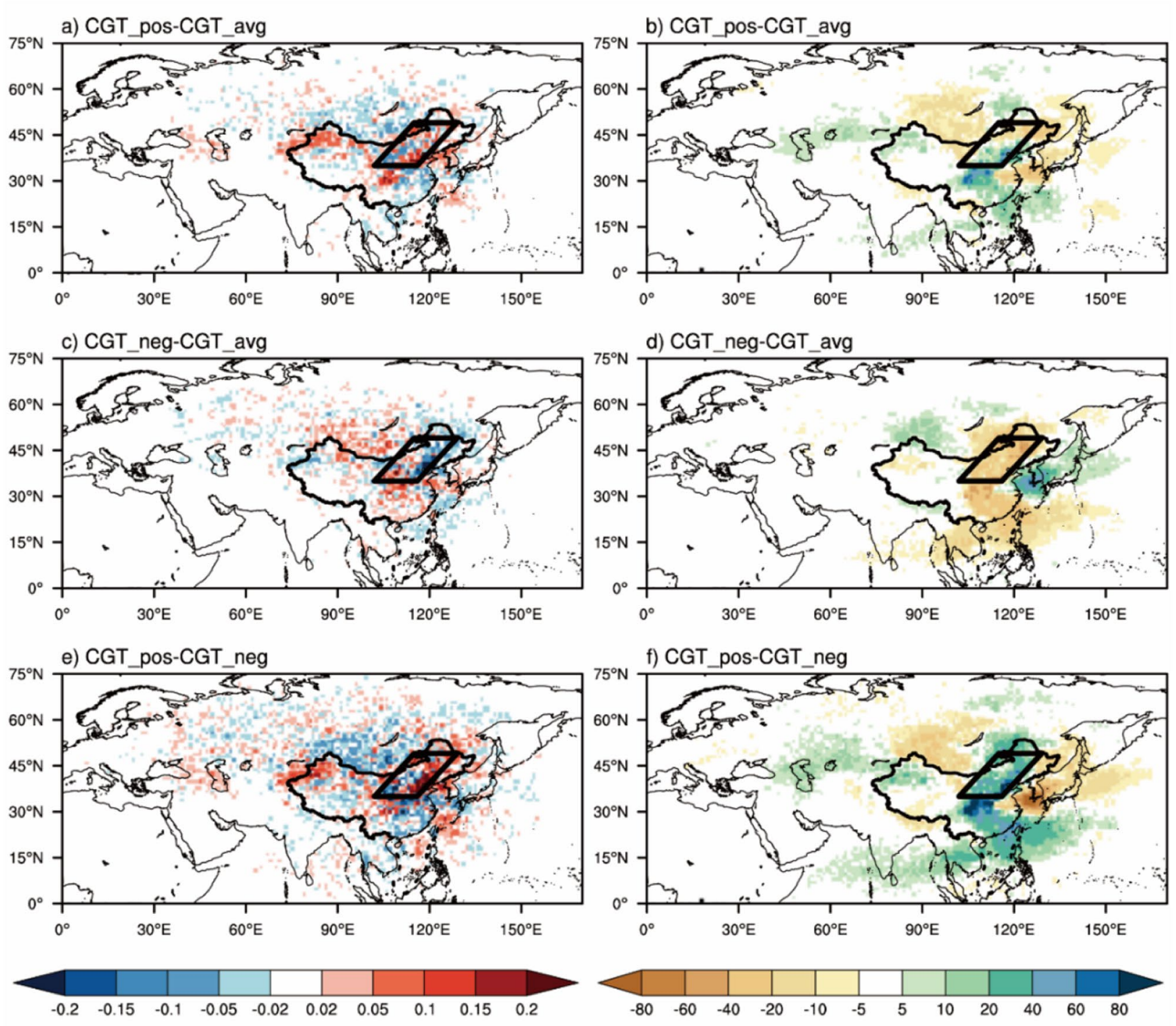

Fig. 13 Same as Fig. 7, but for CGTI

comprising the contribution to precipitation in TCZ will be disclosed, as shown in Fig. 15. During the CGT positive phase years, the water vapor uptake over the monsoon system dominant area increases the most of up to 1.82×10^{14} kg. However, due to the remarkable loss during the transport (1.39×10^{14} kg), the actual contribution increment is 0.36×10^{14} kg. In comparison to monsoon behavior, the local contribution reveals that despite only 0.33×10^{14} kg increase of moisture uptake, the increment of local water vapor contribution is still considerable (0.2×10^{14} kg), because of little loss (0.01×10^{14} kg). Finally, the uptake and loss along the westerlies tend to cancel out each other, and the net effect is negligible (Fig. 13f).

In short, the main mechanisms of CGT affecting the interannual variability of summer precipitation in TCZ also can be concluded as two points: in the positive phase of CGT, distinguishing ascending motion and enhanced moisture supply from summer monsoon and local evaporation.

4 Conclusions and discussion

Eurasia Teleconnection and Circumglobal teleconnection are identified as the main atmospheric teleconnection modes affecting the interannual variability of summer precipitation of transitional climate zone in east Asia. It is worth pointing out that the corresponding indices of the two modes are not significantly correlated on the interannual scale. Therefore, in this study, the underlying physical mechanisms of above two wave train patterns on summer precipitation in the transition zone are separately revealed, based on the

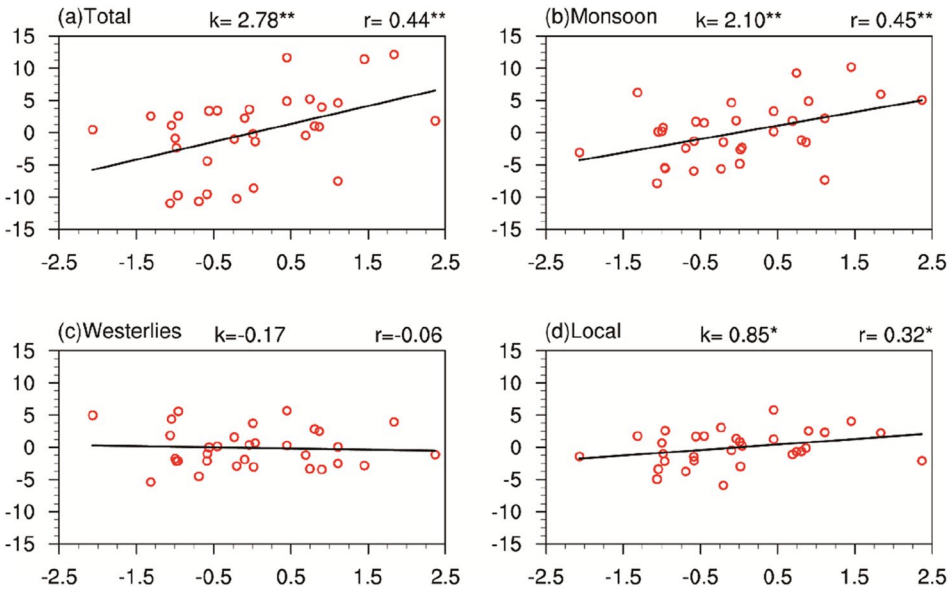

Fig. 14 Same as Fig. 8, but for CGTI

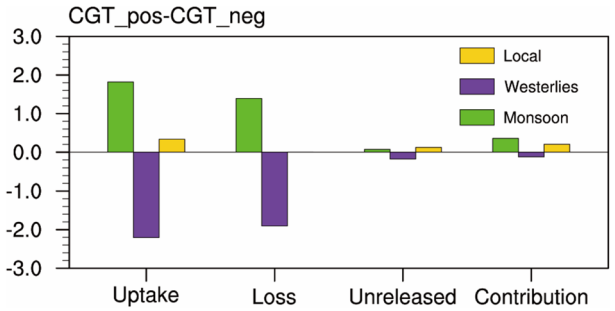

Fig. 15 Same as Fig. 9, but for CGTI

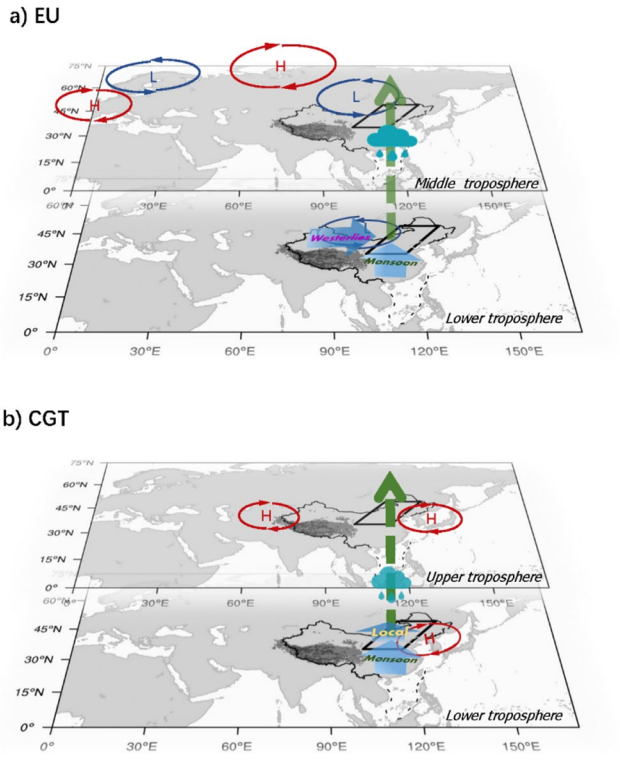

Fig. 16 Physical mechanism of EU teleconnection (**a**) and CGT pattern (**b**) on interannual variability of summer precipitation in TCZ. Blue arrows represent increased water vapor supply from the corresponding system to TCZ, green arrows represent vertical velocity, and red and blue arrows represent circulation anomalies

results of Lagrangian diagnosis combined with the circulation characteristics.

The EU teleconnection mode is a teleconnection wave train propagating from west to east over Eurasia. When in a positive mode, there is a "+-+-" anomalous pressure pattern from Western Europe to Inner Mongolia, as demonstrated in Fig. 16a. This equivalent barotropic structure, on the one hand, is responsible for the low pressure anomaly in the lower troposphere in TCZ and Mongolia region. It not only enhanced the water vapor transport along with mid-latitude westerlies, but also is accompanied by the south wind anomaly, leading to a huge moisture increase from summer monsoon circulation. On the other hand, the negative pressure anomaly also induced anomalous ascending over TCZ by causing abnormal vertical distribution of vertical vorticity advection as well as the worm advections in mid-upper troposphere over TCZ.

CGT, which is positioned within a waveguide associated with the westerly jet stream, is also identified as a source of interannual variability of summer rainfall in TCZ. In the positive CGT phase, upper troposphere over Asian is featured by two positive pressure anomalies in the west side of the Tibetan Plateau and the east China Sea and the Sea of Japan (Fig. 16b), and the latter shows an equivalent barotropic structure

(Enomoto et al. 2003, Ding et al. 2011, Wang et al. 2013). It is suggested that the greatest water vapor increase comes from monsoon system circulations increase, followed by moisture from local evaporation contribution in TCZ during the positive CGT years. In addition, the enhancive updraft induced by vertical vorticity advection anomalies and temperature advection anomalies provides triggering mechanism for accessorial moisture turning to precipitation. It is worth noting that the diabatic heating is not taken into consideration during vertical motion diagnosis of this study. However, the increased precipitation can introduce anomalous diabatic heating, which, in turn, can also strengthen the upward motion (Hu et al. 2017, Gu et al. 2018). Therefore, the positive feedback mechanism between precipitation and upward motion and its roles in wet/dry condition of TCZ deserves further investigation.

Acknowledgements We thank the editor and three anonymous reviewers for their continuous support which helped in improving the manuscript. FLEXPART_10.4 used for particle tracking and moisture analysis was provided freely (downloaded from https://www.flexpart.eu/wiki/FpRoadmap). All data sources are also duly acknowledged.

Author contributions QW: conceptualization; data curation; formal analysis; investigation; methodology; resources; software; visualization; writing—original draft. LW: conceptualization; formal analysis; funding acquisition; project administration; investigation; resources; supervision; writing—review and editing. GH: conceptualization; funding acquisition; resources; supervision; investigation; methodology; writing—review and editing. TW: data curation; validation; writing—review and editing.

Funding This work was supported by the National Natural Science Foundation of China Grants Nos. 41875115, 41961144016, 42175041, 42230605 and 41831175, STEP (2019QZKK0102) and Key Deployment Project of Centre for Ocean Mega-Research of Science, Chinese Academy of Sciences (COMS2019Q03).

Data availability Japanese 55-year Reanalysis dataset (JRA-55) are derived from http://search.diasjp.net/en/dataset/JRA55. The FLEXPART model input data, NCEP–CFSR 6-hourly forecast data dataset, are available online (http://rda.ucar.edu/datasets/ds093.0/). The daily observation precipitation data, provided by the National Meteorological Information Center of the China Meteorological Administration (CMA) can be retrieved on https://data.cma.cn/.

Declarations

Conflict of interest The authors have no relevant financial or non-financial interests to disclose.

Ethics approval and consent to participate Not applicable.

Consent for publication Not applicable.

References

Bin C, Xiang-De X, Tianliang Z (2013) Main moisture sources affecting lower Yangtze River Basin in boreal summers during 2004–2009. Int J Climatol 33(4):1035–1046

Bjerknes J (1969) Atmospheric teleconnections from the equatorial Pacific. Mon Weather Rev 97:163–172

Chen J, Wei H, Jin LY, Chen JH, Chen SQ, Chen FH (2018) A climatological northern boundary index for the east asian summer monsoon and its interannual variability. Sci China-Earth Sci 61(1):13–22

Chen W, Wang L, Feng J, Wen ZP, Ma TJ, Yang XQ, Wang CH (2019) Recent progress in studies of the variabilities and mechanisms of the east asian monsoon in a changing climate. Adv Atmos Sci 36(9):887–901

Chou C, Neelin JD, Chen CA, Tu JY (2009) Evaluating the "Rich-Get-richer'' mechanism in tropical precipitation change under global warming. J Clim 22(8):1982–2005

Dai A (2012) Increasing drought under global warming in observations and models. Nat Clim Change 3(1):52–58

Ding QH, Wang B (2005) Circumglobal teleconnection in the Northern Hemisphere summer. J Clim 18(17):3483–3505

Ding Q, Wang B, Wallace JM, Branstator G (2011) Tropical–extratropical teleconnections in Boreal summer: observed interannual variability. J Clim 24(7):1878–1896

Enomoto T, Hoskins BJ, Matsuda Y (2003) The formation mechanism of the Bonin high in August. Q J R Meteorol Soc 129(587):157–178

Gu W, Wang L, Hu Z-Z, Hu K, Li Y (2018) Interannual variations of the first rainy season precipitation over South China. J Clim 31(2):623–640

Guan XD, Ma JR, Huang JP, Huang RX, Zhang L, Ma ZG (2019) Impact of oceans on climate change in drylands. Sci China-Earth Sci 62(6):891–908

Hao Y, Zhihong J, Zhengyu L, Qiang Z (2014) Analysis of climatic characteristics of water vapor transport based on the lagrangian method: a comparison between Meiyu in the Yangtze – Huaihe River region and the Huaibei rainy season. Chin J Atmos Sci 38(5):965–973

Harada Y, Kamahori H, Kobayashi C, Endo H, Kobayashi S, Ota Y, Onoda H, Onogi K, Miyaoka K, Takahashi K (2016) The JRA-55 reanalysis: representation of atmospheric circulation and climate variability. J Meteorol Soc Jpn 94(3):269–302

Hu K, Xie S-P, Huang G (2017) Orographically anchored El Niño effect on summer rainfall in Central China. J Clim 30(24):10037–10045

Huang G (2004) An index measuring the interannual variation of the east asian summer monsoon—the EAP index. Adv Atmos Sci 21(1):41–52

Huang YJ, Cui XP (2015) Moisture sources of an extreme precipitation event in Sichuan, China, based on the lagrangian method. Atmos Sci Lett 16(2):177–183

Huang G, Liu Y, Huang RH (2011) The interannual variability of summer rainfall in the arid and semiarid regions of Northern China and its association with the Northern Hemisphere circumglobal teleconnection. Adv Atmos Sci 28(2):257–268

Huang J, Guan X, Ji F (2012a) Enhanced cold-season warming in semi-arid regions. Atmos Chem Phys 12(12):5391–5398

Huang R, Liu Y, Feng T (2012b) Interdecadal change of summer precipitation over Eastern China around the late-1990s and associated circulation anomalies, internal dynamical causes. Chin Sci Bull 58(12):1339–1349

Huang J, Li Y, Fu C, Chen F, Fu Q, Dai A, Shinoda M, Ma Z, Guo W, Li Z, Zhang L, Liu Y, Yu H, He Y, Xie Y, Guan X, Ji M, Lin L, Wang S, Yan H, Wang G (2017) Dryland climate change: recent progress and challenges. Rev Geophys 55(3):719–778

Huang JP, Ma JR, Guan XD, Li Y, He YL (2019) Progress in semi-arid climate change studies in China. Adv Atmos Sci 36(9):922–937

Huang JP, Zhang GL, Zhang YT, Guan XD, Wei Y, Guo RX (2020) Global desertification vulnerability to climate change and human activities. Land Degrad Dev 31(11):1380–1391

Iwao K, Takahashi M (2006) Interannual change in summertime precipitation over northeast Asia. Geophys Res Lett 33(16):L16703
James P, Stohl A, Spichtinger N, Eckhardt S, Forster C (2004) Climatological aspects of the extreme european rainfall of August 2002 and a trajectory method for estimating the associated evaporative source regions. Nat Hazards Earth Syst Sci 4(5–6):733–746
Jie W, Qingyun Z, Shiyan T (2004) Physical causes of the1999 and 2000 summer severe drought in North China. Chin J Atmos Sci 28(1):125–137
Kobayashi S, Ota Y, Harada Y, Ebita A, Moriya M, Onoda H, Onogi K, Kamahori H, Kobayashi C, Endo H, Miyaoka K, Takahashi K (2015) The JRA-55 reanalysis: general specifications and basic characteristics. J Meteorol Soc Jpn 93(1):5–48
Kosaka Y, Nakamura H (2010) Mechanisms of meridional teleconnection observed between a summer monsoon system and a subtropical anticyclone. Part I: the Pacific–Japan pattern. J Clim 23(19):5085–5108
Kosaka Y, Xie SP, Nakamura H (2011) Dynamics of interannual variability in summer precipitation over East Asia. J Clim 24(20):5435–5453
Kubota H, Kosaka Y, Xie SP (2015) A 117-year long index of the Pacific-Japan pattern with application to interdecadal variability. Int J Climatol 36(4):1575–1589
Li T, Ling J, Hsu P-C (2020) Madden-Julian oscillation: its discovery, dynamics, and impact on East Asia. J Meteorol Res 34(1):20–42
Lin ZD, Bueh C (2022) Interannual variability of the east asian trough in summer. Clim Dyn
Liu Y, Wang L, Zhou W, Chen W (2014) Three eurasian teleconnection patterns: spatial structures, temporal variability, and associated winter climate anomalies. Clim Dyn 42(11–12):2817–2839
Lu W, Jia GS (2013) Fluctuation of farming-pastoral ecotone in association with changing East Asia monsoon climate. Clim Change 119(3–4):747–760
Madden RA, Julian PR (1971) Detection of a 40–50 day oscillation in the Zonal wind in the Tropical Pacific. J Atmos Sci 29:702–708
Ming J, Sun J, Yu S (2019) Combined impact of the Pacific–Japan pattern and Mediterranean–northern Eurasia pattern on east asian summer temperatures. Atmos Ocean Sci Lett 12(3):208–217
North GR, Bell TL, Cahalan RF, Moeng FJ (1982) Sampling errors in the estimation of empirical orthogonal functions. Mon Weather Rev 110:699–706
Numaguti A (1999) Origin and recycling processes of precipitating water over the Eurasian continent: experiments using an atmospheric general circulation model. J Geophys Res Atmos 104(D2):1957–1972
Ou TH, Qian WH (2006) Vegetation variations along the monsoon boundary zone in East Asia. Chin J Geophys-Chinese Ed 49(3):698–705
Piao JL, Chen W, Wei K, Liu Y, Graf HF, Ahn JB, Pogoreltsev A (2017) An abrupt rainfall decrease over the asian inland plateau region around 1999 and the possible underlying mechanism. Adv Atmos Sci 34(4):456–468
Piao JL, Chen W, Chen SF, Gong HN, Zhang Q (2020) Summer water vapor sources in Northeast Asia and East Siberia revealed by a moisture-tracing atmospheric model. J Clim 33(9):3883–3899
Piao JL, Chen W, Chen SF (2021) Water vapour transport changes associated with the interdecadal decrease in the summer rainfall over Northeast Asia around the late-1990s. Int J Climatol 41(S1):E1469–E1482
Piao JL, Chen W, Wang L, Chen SF (2022) Future projections of precipitation, surface temperatures and drought events over the monsoon transitional zone in China from bias-corrected CMIP6 models. Int J Climatol 42(2):1203–1219
Saha S, Moorthi S, Pan HL, Wu XR, Wang JD, Nadiga S, Tripp P, Kistler R, Woollen J, Behringer D, Liu HX, Stokes D, Grumbine R, Gayno G, Wang J, Hou YT, Chuang HY, Juang HMH, Sela J, Iredell M, Treadon R, Kleist D, Van Delst P, Keyser D, Derber J, Ek M, Meng J, Wei HL, Yang RQ, Lord S, Van den Dool H, Kumar A, Wang WQ, Long C, Chelliah M, Xue Y, Huang BY, Schemm JK, Ebisuzaki W, Lin R, Xie PP, Chen MY, Zhou ST, Higgins W, Zou CZ, Liu QH, Chen Y, Han Y, Cucurull L, Reynolds RW, Rutledge G, Goldberg M (2010) The Ncep climate forecast system reanalysis. Bull Am Meteorol Soc 91(8):1015–1057
Salih AAM, Zhang Q, Tjernstrom M (2015) Lagrangian tracing of Sahelian Sudan moisture sources. J Geophys Res-Atmos 120(14):6793–6808
Seager R, Naik N, Vecchi GA (2010) Thermodynamic and dynamic mechanisms for large-scale changes in the hydrological cycle in response to global warming. J Clim 23(17):4651–4668
Sodemann H, Schwierz C, Wernli H (2008) Interannual variability of Greenland winter precipitation sources: lagrangian moisture diagnostic and north Atlantic Oscillation influence. J Geophys Res-Atmos 113:D03107
Stohl A, James P (2004) A lagrangian analysis of the atmospheric branch of the global water cycle. Part I: method description, validation, and demonstration for the August 2002 flooding in central Europe. J Hydrometeorol 5(4):656–678
Sun B, Wang HJ (2014) Moisture sources of semiarid grassland in China using the Lagrangian particle model FLEXPART. J Clim 27(6):2457–2474
Sun B, Wang HJ (2015) Analysis of the major atmospheric moisture sources affecting three sub-regions of East China. Int J Climatol 35(9):2243–2257
Takaya K, Nakamura H (2001) A formulation of a phase-independent wave-activity flux for stationary and migratory quasigeostrophic eddies on a zonally varying basic flow. J Atmos Sci 58(6):608–627
Wakabayashi S, Kawamura R (2004) Extraction of major teleconnection patterns possibly associated with the anomalous summer climate in Japan. J Meteorol Soc Jpn 82(6):1577–1588
Wallace JM, Gutzler DS (1981) Teleconnections in the geopotential height field during the Northern Hemisphere winter. Mon Weather Rev 109(4):784–812
Wang H, He S (2015) The North China/Northeastern asia severe summer drought in 2014. J Clim 28(17):6667–6681
Wang H, Li DL (2011) Correlation of surface sensible heat flux in the arid region of northwestern China with the northern boundary of the east asian summer monsoon and chinese summer precipitation. J Geophys Res-Atmos 116:D19
Wang C, Deser C, Yu J-Y, DiNezio P, Clement A (2017a) El Niño and Southern Oscillation (ENSO): a review. In: Coral Reefs of the Eastern Tropical Pacific, pp 85–106
Wang L, Xu PQ, Chen W, Liu Y (2017b) Interdecadal variations of the silk road pattern. J Clim 30(24):9915–9932
Wang WW, Zhou W, Wang X, Fong SK, Leong KC (2013) Summer high temperature extremes in Southeast China associated with the east asian jet stream and circumglobal teleconnection. J Geophys Res-Atmos 118(15):8306–8319
Wang QL, Wang L, Huang G, Piao JL, Chotamonsak C (2021) Temporal and spatial variation of the transitional climate zone in summer during 1961–2018. Int J Climatol 41(3):1633–1648
Wang Q, Huang G, Wang L, Piao J, Ma T, Hu P, Chotamonsak C, Limsakul A (2022) Mechanism of the summer rainfall variation in transitional climate zone in East Asia from the perspective of moisture supply during 1979–2010 based on the Lagrangian method. Clim Dyn
Xu ZQ, Fan K, Wang HJ (2015) Decadal variation of summer precipitation over China and associated atmospheric circulation after the late 1990s. J Clim 28(10):4086–4106
Xu Y, Zhao P, Si D, Cao L, Wu X, Zhao Y, Liu N (2019) Development and preliminary application of a gridded surface air

temperature homogenized dataset for China. Theoret Appl Climatol 139(1–2):505–516
Xu P, Wang L, Ming J (2022) Central asian precipitation extremes affected by an intraseasonal planetary wave pattern. J Clim 35(8):2603–2616
Zhang RN, Sun CH, Li WJ (2018) Relationship between the interannual variations of Arctic sea ice and summer eurasian teleconnection and associated influence on summer precipitation over China. Chin J Geophys 61:91–105
Zhao W, Chen W, Chen SF, Yao SL, Nath D (2019) Inter-annual variations of precipitation over the monsoon transitional zone in China during August-September: role of sea surface temperature anomalies over the tropical Pacific and North Atlantic. Atmos Sci Lett 20(1):e872
Zhao W, Chen W, Chen SF, Nath D, Wang L (2020) Interdecadal change in the impact of North Atlantic SST on August rainfall over the monsoon transitional belt in China around the late 1990s. Theoret Appl Climatol 140(1–2):503–516
Zhou S, Huang G, Huang P (2017) Changes in the east asian summer monsoon rainfall under global warming: moisture budget decompositions and the sources of uncertainty. Clim Dyn 51(4):1363–1373

Publisher's Note Springer Nature remains neutral with regard to jurisdictional claims in published maps and institutional affiliations.

Springer Nature or its licensor (e.g. a society or other partner) holds exclusive rights to this article under a publishing agreement with the author(s) or other rightsholder(s); author self-archiving of the accepted manuscript version of this article is solely governed by the terms of such publishing agreement and applicable law.